Design and Implementation of a Nine-Axis Inertial Measurement Unit

Pei-Chun Lin, *Member, IEEE*, Jau-Ching Lu, Chia-Hung Tsai, and Chi-Wei Ho

***Abstract*—A nine-axis inertial measurement unit (IMU) that utilizes three-axis angular velocity measurements from rate gyroscopes and six-axis linear acceleration measurements from three two-axis accelerometers is reported. This system can derive linear acceleration, angular acceleration, and angular velocity via simple memoryless matrix operations, and eliminates the requirement for accelerometer installation at the center of mass as in the traditional IMU. An optimal configuration of the system is proposed based on the analysis of rigid body dynamics and matrix theory. In this configuration, the computed angular acceleration is free of the gravity effect as well. Analyses of sensor position and orientation errors are reported. Experimental validation was executed to evaluate the performance of the system.**

***Index Terms*—Accelerometer, body state, gyroscope, inertial measurement unit (IMU).**

I. Introduction

FOR several decades, inertial sensors [1] have been one of the important categories of sensors utilized in various applications, including navigation (robots [2], [3] and vehicles [4], [5]), state estimation for motion analysis [6], [7] or dynamic modeling, motion control [8]–[11], microsurgery [12], rehabilitation [13]–[15], and avoiding sports injury [16], [17]. In modeling dynamics of the legged robots [18], [19], information about external forces, position, and orientation states (including their first and second derivatives) is usually required as essential information for constructing second-order dynamic models, and inertial sensors are appropriate choices to provide some essential information about these states. Traditionally, a standard inertial measurement unit (IMU) composed of a three-axis accelerometer installed at center of mass (COM) and a three-axis rate gyroscope (hereafter referred to as the "gyro") readily provide measurements of linear acceleration and angular velocity, accordingly. Though full position/orientation state can be reconstructed by models and filter technologies such as the Kalman filter, such systems usually yield poor performance and generate unbounded integration errors due to the nature of their unobservability [19]. Thus, techniques of fusing IMU with other positioning sensors (GPS [20], magnetocompass [21], laser [22], and vision system [23]) are widely adapted. While linear displacement, velocity, and acceleration, as well as orientation and angular velocity, can all be measured by commercially available sensors, the only immeasurable is angular acceleration. Though this information can be derived by differentiation of gyro signals, it is usually noisy. Therefore, besides improving the performance of the gyros and associated data acquisition systems, searching for new techniques that are capable of yielding reliable and accurate angular acceleration states plays a nontrivial role in the development of IMUs.

In rigid body dynamics, linear accelerations of any two points on the body, as well as angular acceleration and angular velocity of the body, are related to a specific mathematical equation based on the Newton mechanics. Since the linear acceleration and the angular velocity can be measured directly by the accelerometers and the gyros, the angular acceleration can readily be derived by utilizing these measurements together with the Newtonian equation. For decades, researchers have evaluated various methods in an attempt to recover all three states via a minimum set of sensors together with specific computational algorithms. Among all of these, development of accelerometer-based systems is one widely adopted method. Padgaonkar *et al.* [24] proposed a nine-axis acceleration measurement system capable of deriving bounded linear and angular acceleration but with limited angular velocity information. Chen *et al*. [25] proposed a novel six-axis system that shifted the unavoidable integration computation to linear acceleration; thus, the bounded angular acceleration can be derived. Genin *et al.* [26] reported angular velocity determination from accelerometer measurements. Angeles *et al.* [27] proposed various nice body state estimation methods from point acceleration measurements. Parsa *et al.* [28] developed an all-accelerometer IMU that requires 12 one-axis accelerometers mounted at distinct and specific locations on the surfaces of a cube, and the system is capable of deriving all nine unknown scalar states. Recently, with the advanced development in microelectrical mechanical systems (MEMSs), multiaxis MEMS inertial sensors have become commercially available and low cost, yet with promising performance.[1] Particularly, the appearances of the MEMS gyros, which readily provide an angular velocity state, eliminate the inverse of quadratic computations required in all-accelerometer IMUs. This motivates us to revisit the question of how to select, place, and orient inertial sensors in order to yield better performance and feasible solutions for practical implementation.

Manuscript received October 25, 2010; revised December 15, 2010; accepted January 7, 2011. Recommended by Technical Editor D. Sun. This work was supported in part by the National Science Council (NSC), Taiwan, under Contract NSC 97-2221-E-002-208-MY3. This paper was presented in part at the IEEE International Conference on Robotics and Automation, Kobe, Japan, May 2009.

P.-C. Lin, J.-C. Lu, and C.-H. Tsai are with the Department of Mechanical Engineering, National Taiwan University, Taipei 10617, Taiwan (e-mail: peichunlin@ntu.edu.tw).

C.-W. Ho was with the Department of Mechanical Engineering, National Taiwan University, Taipei 10617, Taiwan. He is now with the Department of Automation Development, HTC, Taoyuan 330, Taiwan.

Digital Object Identifier 10.1109/TMECH.2011.2111378

[1]For example, Analog Devices, Inc., Freescale Semiconductor, VTI Technologies, Measurement Specialties, Inc./Schaevitz, and STMicroelectronics all produce three-axis MEMS accelerometers. InvenSense and STMicroelectronics produce three-axis MEMS gyroscopes.

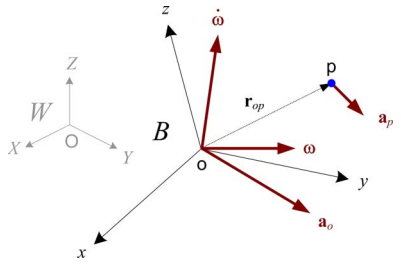

Fig. 1. Acceleration of a point p in an accelerating body frame B is determined by the position vector from the origin of B to p and the states of the body frame B with respect to the inertial frame W.

Here, we investigate a nine-axis IMU containing three-axis angular velocity measurements from the gyros and six-axis linear acceleration measurements from the accelerometers positioned at three distinct locations. This nine-axis IMU provides angular acceleration derivation via memoryless linear operation, unlike the differentiation process utilized in the traditional IMU, which requires a sequence of data with high sampling rate. The flexible positioning of three two-axis accelerometers in the system obviates the strong constraint of accelerometer installation at COM as in the traditional IMU. The use of a three-axis gyro readily provides angular velocity that eliminates the procedure of deriving the state from its quadratic forms as in an all-accelerometer IMU [29]. In addition, the angular velocity and acceleration derived by the system are both free of gravity effect as well.

Section II introduces the idea of this nine-axis sensory system based on an analysis of rigid body dynamics, followed by Section III, which describes the positioning of sensors in detail. Section IV presents an analysis of sensor position and orientation error. Section V reports the results of experimental evaluation, and Section VI concludes the paper.

II. Construction of the Sensing System

As shown in Fig. 1, the acceleration vector $\mathbf{a}_p$ of a point p rigidly attached to an accelerating body frame B with origin o in the inertial frame W is a function of the body's angular velocity $\boldsymbol{\omega}$, angular acceleration $\dot{\boldsymbol{\omega}}$, and linear acceleration of the body origin $\mathbf{a}_o$, given by

$$\mathbf{a}_p = \mathbf{a}_o + \dot{\boldsymbol{\omega}} \times \mathbf{r}_{op} + \boldsymbol{\omega} \times (\boldsymbol{\omega} \times \mathbf{r}_{op}) \tag{1}$$

where $\mathbf{r}_{op}$, the fixed position vector of point p relative to o, is presumed known *a priori*. In general, we are interested in utilizing the measurements from commercially available accelerometers and gyros to derive nine unknown scalar body states on the right side of the equation, including the COM linear acceleration $\mathbf{a}_{\mathrm{COM}}$ (usually equal to the origin of body frame $\mathbf{a}_o$)

$$\mathbf{a}_o = \mathbf{a}_{\mathrm{COM}} = [a_x \quad a_y \quad a_z]^T \tag{2a}$$

and the angular acceleration and velocity

$$\dot{\boldsymbol{\omega}} = [\dot{\omega}_x \quad \dot{\omega}_y \quad \dot{\omega}_z]^T \tag{2b}$$

$$\boldsymbol{\omega} = [\omega_x \quad \omega_y \quad \omega_z]^T. \tag{2c}$$

A quadratic representation of angular velocity $\boldsymbol{\omega}_6$ is also defined as

$$\boldsymbol{\omega}_6(\boldsymbol{\omega}) = \begin{bmatrix} \omega_x^2+\omega_y^2 & \omega_x^2+\omega_z^2 & \omega_y^2+\omega_z^2 & \omega_x\omega_y \\ \omega_x\omega_z & \omega_y\omega_z \end{bmatrix}^T. \tag{2d}$$

The ith one-axis gyro installed on the body measures the projected angular velocity of spatial body motion, ω_i, along the sensing direction $\hat{\boldsymbol{s}}_{\mathbf{g}\_i}$

$${}^b\omega_i = \boldsymbol{\omega}^T \cdot \hat{\boldsymbol{s}}_{\mathbf{g}\_i} \tag{3a}$$

where the sensed motion is with respect to the inertial frame, but the coordinates are represented in the body frame (i.e., letter "b" on the upper left corner of the state). Likewise, the jth one-axis accelerometer installed at point p on the body measures the projected linear acceleration along the sensing direction $\hat{\boldsymbol{s}}_{\mathbf{a}\_j}$

$$\begin{aligned} {}^b a_j &= \mathbf{a}_p^T \cdot \hat{\boldsymbol{s}}_{\mathbf{a}\_j} \\ &= (\mathbf{a}_o + \dot{\boldsymbol{\omega}} \times \mathbf{r}_{op} + \boldsymbol{\omega} \times (\boldsymbol{\omega} \times \mathbf{r}_{op}))^T \cdot \hat{\boldsymbol{s}}_{\mathbf{a}\_j}. \end{aligned} \tag{3b}$$

Here, the gravity-induced acceleration is presumably compensated for the measurement of the accelerometer.

Since the position vector $\mathbf{r}_{op}$ and the sensing direction $\hat{\boldsymbol{s}}_{\mathbf{g}\_i}$ or $\hat{\boldsymbol{s}}_{\mathbf{a}\_j}$ are invariant with respect to the body frame B in a general strapdown IMU, it motivates us to express the coordinates of dynamic equation (1) in the body frame at every instance

$${}^b\mathbf{a}_p - {}^b\boldsymbol{\omega} \times ({}^b\boldsymbol{\omega} \times {}^b\mathbf{r}_{op}) = {}^b\mathbf{a}_o + {}^b\dot{\boldsymbol{\omega}} \times {}^b\mathbf{r}_{op} \tag{4}$$

while the measured states of the moving rigid body are still with respect to the initial frame. Note that in the following content, all the equations will be expressed in the body coordinates, and all instances of notation "b" will be omitted for clear equation presentations.

Presumably, we have six one-axis gravity-compensated linear acceleration measurements from the accelerometers

$$\mathbf{a}_{\mathbf{m}} = [a_1 \quad a_2 \quad a_3 \quad a_4 \quad a_5 \quad a_6]^T \tag{5a}$$

and three one-axis angular velocity measurements from the gyros

$$\boldsymbol{\omega}_{\mathbf{m}} = [\omega_1 \quad \omega_2 \quad \omega_3]^T \tag{5b}$$

with known sensor positions and orientations $\hat{\boldsymbol{s}}_{\mathbf{g}\_i}$ or $\hat{\boldsymbol{s}}_{\mathbf{a}\_j}$ on the body; six scalar versions of (4) can be constructed and the left side of (4) is known. Consequently, the remaining six unknown acceleration states on the right side

$$\mathbf{x}_{\mathrm{var}} = [\mathbf{a}_o^T \quad \dot{\boldsymbol{\omega}}^T]^T = [\ a_x \quad a_y \quad a_z \quad \dot{\omega}_x \quad \dot{\omega}_y \quad \dot{\omega}_z\ ]^T \tag{6}$$

with respect to the inertial frame can be derived by simple linear computation. This procedure completes the computation of the desired body state that we will proceed to detail.

Without loss of generality, we can arrange the sensing directions of three one-axis gyros, $\hat{\boldsymbol{s}}_{\mathbf{g}\_i\ i=1,2,3}$, aligned with three principal axes of the body frame B

$$\hat{\boldsymbol{s}}_{\mathbf{g}\_1} = [1 \quad 0 \quad 0]^T \qquad \hat{\boldsymbol{s}}_{\mathbf{g}\_2} = [0 \quad 1 \quad 0]^T$$
$$\hat{\boldsymbol{s}}_{\mathbf{g}\_3} = [0 \quad 0 \quad 1]^T. \tag{7}$$

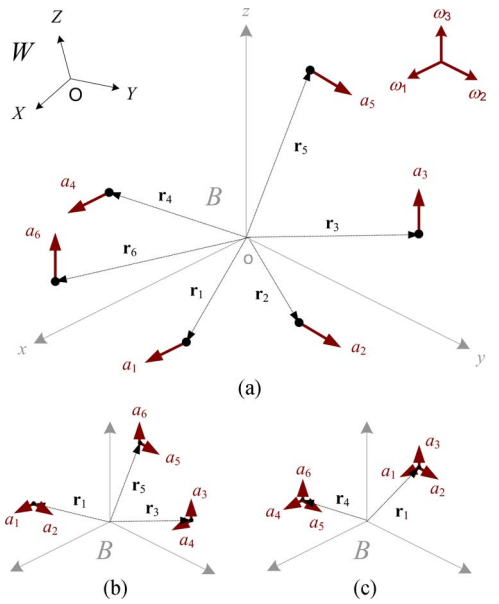

Fig. 2. Three different arrangements of six one-axis acceleration measurements. (a) Six one-axis measurements at six distinct locations. (b) Three two-axis measurements at three distinct locations. (c) Two three-axis measurements at two distinct locations.

In this arrangement, output of the gyros readily represents one of the desired body states: angular velocity

$$\boldsymbol{\omega} = \boldsymbol{\omega}_{\mathbf{m}} \tag{8}$$

and the coordinates are expressed in the body frame. The direct measurement of angular velocity from readings of gyros obviates the quadratic computation and equation solving in real-time operation as in the all-accelerometer system in which this state is, in general, treated as unknown.

By using a similar strategy, six one-axis accelerometers can be oriented to measure the linear accelerations $\mathbf{a}_{\mathbf{m}}$ along with the three principal axes of body frame B as well, with each axis having two measurements for symmetric considerations. Instead of the inner product computations described in (3a) and (3b), computation in the current settings only requires selecting one out of three scalar components of the dynamic equation, as shown in (4).

Now, the question becomes how to place these six one-axis accelerometers so that the remaining unknown state $\mathbf{x}_{\text{var}}$ can be derived successfully. Without loss of generality, assume that: 1) the locations of six one-axis accelerometers are defined by six position vectors

$$\begin{aligned} \mathbf{r} &= [\ \mathbf{r}_1 \quad \mathbf{r}_2 \quad \mathbf{r}_3 \quad \mathbf{r}_4 \quad \mathbf{r}_5 \quad \mathbf{r}_6\ ] \\ \mathbf{r}_j &= [\, r_{jx} \quad r_{jy} \quad r_{jz}]^T_{j\,=\,1-6} \end{aligned} \tag{9}$$

where $\mathbf{r}_j$ behaves the same as $\mathbf{r}_{op}$ defined in (4), and 2) the sensing directions of these six sensors are alongside x, y, z, x, y, and z principal axes of the body frame B, respectively [as shown in Fig. 2(a)]. Thus, the left side of (4) can be readily computed with sensor measurements $\mathbf{a}_{\mathbf{m}}$ and $\omega_{\mathbf{m}}$

$$\begin{aligned} &q_j = a_j - (\boldsymbol{\omega}_{\mathbf{m}} \times (\boldsymbol{\omega}_{\mathbf{m}} \times \mathbf{r}_j))^T \cdot \hat{\mathbf{e}}_k \quad {\scriptstyle j=1\text{–}6, k=x,y,z,x,y,z} \\ &\mathbf{q} = [\ q_1 \quad q_2 \quad q_3 \quad q_4 \quad q_5 \quad q_6\ ]^T = \mathbf{a}_{\mathbf{m}} - \mathbf{W}(\mathbf{r})\boldsymbol{\omega}_6(\boldsymbol{\omega}_{\mathbf{m}}) \end{aligned}$$

$$= \begin{bmatrix} a_1 \\ a_2 \\ a_3 \\ a_4 \\ a_5 \\ a_6 \end{bmatrix} - \begin{bmatrix} 0 & 0 & -r_{1x} & r_{1y} & r_{1z} & 0 \\ 0 & -r_{2y} & 0 & r_{2x} & 0 & r_{2z} \\ -r_{3z} & 0 & 0 & 0 & r_{3x} & r_{3y} \\ 0 & 0 & -r_{4x} & r_{4y} & r_{4z} & 0 \\ 0 & -r_{5y} & 0 & r_{5x} & 0 & r_{5z} \\ -r_{6z} & 0 & 0 & 0 & r_{6x} & r_{6y} \end{bmatrix} \begin{bmatrix} \omega_1^2+\omega_2^2 \\ \omega_1^2+\omega_3^2 \\ \omega_2^2+\omega_3^2 \\ \omega_1\omega_2 \\ \omega_1\omega_3 \\ \omega_2\omega_3 \end{bmatrix}. \tag{10}$$

The multiplication of $\mathbf{W}(\mathbf{r})$ and $\boldsymbol{\omega}_6(\boldsymbol{\omega}_{\mathbf{m}})$ is the reorganized form of double cross products between angular velocity and position vectors in which the gyro measurement $\boldsymbol{\omega}_{\mathbf{m}}$ is represented by the 6×1 vector with quadratic representation defined in (2d).

By importing the equations defined in (10) into (4), the linear system of equations can be represented as

$$\mathbf{q} = \mathbf{a}_{\mathbf{m}} - \mathbf{W}(\mathbf{r})\boldsymbol{\omega}_6(\boldsymbol{\omega}_{\mathbf{m}}) = \mathbf{S}(\mathbf{r})\mathbf{x}_{\text{var}} \tag{11}$$

where $\mathbf{S}(\mathbf{r})$ is the 6×6 matrix

$$\mathbf{S}(\mathbf{r}) = \begin{bmatrix} 1 & 0 & 0 & 0 & r_{1z} & -r_{1y} \\ 0 & 1 & 0 & -r_{2z} & 0 & r_{2x} \\ 0 & 0 & 1 & r_{3y} & -r_{3x} & 0 \\ 1 & 0 & 0 & 0 & r_{4z} & -r_{4y} \\ 0 & 1 & 0 & -r_{5z} & 0 & r_{5x} \\ 0 & 0 & 1 & r_{6y} & -r_{6x} & 0 \end{bmatrix}. \tag{12}$$

Thus, the unknown acceleration states can be derived by the matrix operation as follows:

$$\mathbf{x}_{\text{var}} = \mathbf{S}(\mathbf{r})^{-1}(\mathbf{a}_{\mathbf{m}} - \mathbf{W}(\mathbf{r})\boldsymbol{\omega}_6(\boldsymbol{\omega}_{\mathbf{m}})) \tag{13}$$

and this equation reveals that the extraction of the desired acceleration data $\mathbf{x}_{\text{var}}$ now hinges upon the rank and numerical condition of the "structure matrix" $\mathbf{S}(\mathbf{r})$ that is solely a function of positions of accelerometers $\mathbf{r}$. Since the positions are known and fixed in the body coordinates, the following task relies on adequate allocation of accelerometers.

III. Sensor Allocation

The rise of MEMS sensing technology has yielded commercially available low-cost MEMS accelerometers with better performance, lower prices, and smaller packaging than those of a decade ago. More importantly, the availability of multiaxis accelerometers significantly simplifies the original complicated electronic and spatial design of multisensor systems for multiaxis state measurements. Therefore, the spatial allocations of the six one-axis acceleration measurements presented in this paper can be categorized into three different scenarios: 1) two one-axis accelerometers (two $\mathbf{r}_j$s) positioned at two distinct locations; 2) three one-axis accelerometers (three $\mathbf{r}_j$s) positioned at three distinct locations; and 3) six one-axis accelerometers (six $\mathbf{r}_j$s) positioned at six distinct locations. We will discuss these cases separately and focus on the invertibility of the structure matrices $\mathbf{S}(\mathbf{r})$ and their numerical conditions detailed as follows.

A. System With Two Three-Axis Acceleration Measurements

The general spatial configuration of a system with two three-axis acceleration measurements is depicted in Fig. 2(c), where

six position vectors are combined with two distinct position vectors $\mathbf{r}_1$ (=$\mathbf{r}_2$=$\mathbf{r}_3$) and $\mathbf{r}_4$ (= $\mathbf{r}_5$=$\mathbf{r}_6$), containing measurements of $[\,a_1 \quad a_2 \quad a_3\,]^T$ and $[\,a_4 \quad a_5 \quad a_6\,]^T$ accordingly.

The corresponding structure matrix $\mathbf{S}_{2\times3}(\mathbf{r})$ is

$$\mathbf{S}_{2\times3}(\mathbf{r}) = \begin{bmatrix} 1 & 0 & 0 & 0 & r_{1z} & -r_{1y} \\ 0 & 1 & 0 & -r_{1z} & 0 & r_{1x} \\ 0 & 0 & 1 & r_{1y} & -r_{1x} & 0 \\ 1 & 0 & 0 & 0 & r_{4z} & -r_{4y} \\ 0 & 1 & 0 & -r_{4z} & 0 & r_{4x} \\ 0 & 0 & 1 & r_{4y} & -r_{4x} & 0 \end{bmatrix}. \tag{14a}$$

In this case, the structure matrix $\mathbf{S}_{2\times3}(\mathbf{r})$ is composed of two copies of the dynamic equation, as shown in (4). For each copy (upper/lower three rows), the first 3×3 identity matrix corresponds to the computation of the COM linear acceleration, and the second 3×3 skew-symmetric matrix represents the cross product between the position vector and the angular acceleration vector. Unfortunately, the determinant of the structure matrix $\mathbf{S}_{2\times3}(\mathbf{r})$ is always 0, which indicates that the matrix is not invertible and implies that the desired acceleration state $\mathbf{x}_{\text{var}}$ cannot be derived in this configuration. Apparently, six scalar position variables in $\mathbf{r}_1$ and $\mathbf{r}_4$ are not sufficient to construct six independent vectors in the structure matrix.

B. System With Three Two-Axis Acceleration Measurements

By following similar logic to that presented in the previous section, the general spatial configuration of a system with three two-axis acceleration measurements is depicted in Fig. 2(b), where three distinct position vectors $\mathbf{r}_1$ (=$\mathbf{r}_2$), $\mathbf{r}_3$ (=$\mathbf{r}_4$), and $\mathbf{r}_5$ (=$\mathbf{r}_6$) contain measurements of $[\,a_1 \quad a_2\,]^T$, $[\,a_3 \quad a_4\,]^T$, and $[\,a_5 \quad a_6\,]^T$, respectively. In the following development, the three positions are referred as positions I, II, and III, accordingly.

The corresponding structure matrix $\mathbf{S}_{3\times2}(\mathbf{r})$ is

$$\mathbf{S}_{3\times2}(\mathbf{r}) = \begin{bmatrix} 1 & 0 & 0 & 0 & r_{1z} & -r_{1y} \\ 0 & 1 & 0 & -r_{1z} & 0 & r_{1x} \\ 0 & 0 & 1 & r_{3y} & -r_{3x} & 0 \\ 1 & 0 & 0 & 0 & r_{3z} & -r_{3y} \\ 0 & 1 & 0 & -r_{5z} & 0 & r_{5x} \\ 0 & 0 & 1 & r_{5y} & -r_{5x} & 0 \end{bmatrix} \tag{14b}$$

which is a function of nine scalar position variables. In this scenario, the matrix is composed of three copies of two differently selected scalar components of the spatial dynamic equation, as shown in (4). The determinant of this nine-variable structure matrix $\mathbf{S}_{3\times2}(\mathbf{r})$ can be organized as

$$\begin{aligned} \det(\mathbf{S}_{3\times2}(\mathbf{r})) = &-(r_{1x}-r_{5x})(r_{5y}-r_{3y})(r_{3z}-r_{1z}) \\ &-(r_{5x}-r_{3x})(r_{3y}-r_{1y})(r_{1z}-r_{5z}) \end{aligned} \tag{15}$$

and this indicates that the arrangement of sensor positions is crucial in order to avoid singularity of the structure matrix. Geometrically, by considering a triangle formed by the relative position vectors of sensor positions, as shown in Fig. 3, the six terms in (15) represent the components of vectors $\mathbf{r}_{13}$, $\mathbf{r}_{35}$, and $\mathbf{r}_{51}$ projected on the yz, xy, and zx planes, respectively. Various positioning configurations of accelerometers can make the determinant of $\mathbf{S}_{3\times2}(\mathbf{r})$ zero. For example, the positions of the three sensors have the same x, y, or z components—i.e., the

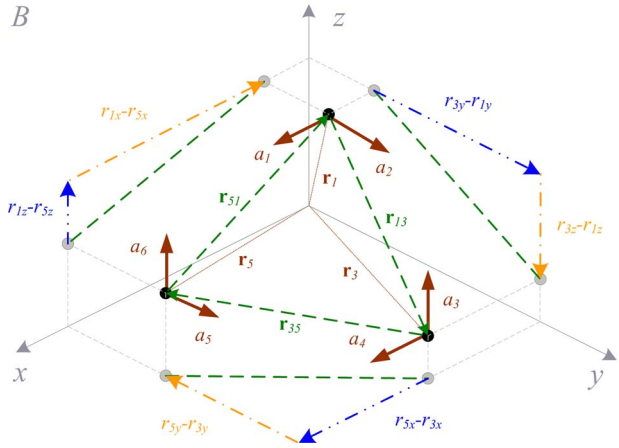

Fig. 3. Geometrical representation of the six vector components appearing in the determinant of the structure matrix (scenario: system with three two-axis accelerometers).

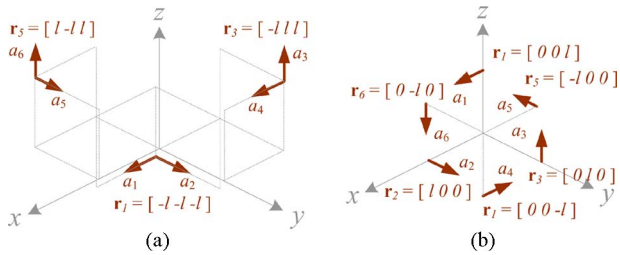

Fig. 4. Configuration of the systems with the best conditioned structure matrices. (a) System with three two-axis measurements at three distinct locations (referred as positions I, II, and III, respectively). (b) System with six one-axis measurements at six distinct locations.

plane composed by the positions of the three sensors (hereafter referred to as the "sensor plane") is parallel to the xy, yz, or zx plane (referred as "sensing plane," the plane spanned by the directions of two sensing vectors at each location). More generally, no matter what the orientations of principal axes are, this phenomenon is also true as long as the sensor plane is parallel to one of three sensing planes.

The condition number of the matrix further indicates the quality of the inversion. The singular values are determined by high-order polynomials (in the entries of the sensor positions $\mathbf{r}$) that are harder to analyze symbolically, but intuitively, the condition number is very sensitive to the "shape" and "magnitude" of the sensor positions relative to each other and their locations relative to the COM. Not surprisingly, the condition number is invariant to rotations of the sensor positions around the COM; hence, the general behavior of condition number versus sensor position can be investigated numerically by moving sensor positions spatially with respect to the current body coordinates. Most likely, the optimal condition occurs when sensors are placed with respect to the COM in certain geometric symmetries. In practice, numerical exploration suggests that the configuration of the three two-axis accelerometers system, as shown in Fig. 4(a), yields the best condition number 2, while the length scale l is located between 0.5–1. Interestingly, because the structure matrix $\mathbf{S}(\mathbf{r})$ combines entries both with and without physical scale in the same rows—"1" in the first 3×3 identity matrix is dimensionless, and the second 3×3 skew-symmetric matrix has a unit of

"length"—it turns out that there is actually a preferred linear dimension of this system at which the resulting condition number is optimal. For example, a physical installation of sensors with $l = 10$ cm should use "decimeter" as the unit that sets $l = 1$, not centimeter ($l = 10$) or meter ($l = 0.1$) that yield large condition numbers 20 and 10, respectively. The condition number of the matrix is determined purely by the relative magnitudes of its matrix elements, thus choosing the right unit so that the magnitudes of the elements close to the optimum condition will reduce the additional error induced by the matrix inversion.

C. System With Six One-Axis Acceleration Measurements

This most general case has been described in Section II and is depicted in Fig. 2(a). The structure matrix of this scenario shown in (12) is a function of 12 scalar position variables. The determinant of structure matrix $\mathbf{S}(\mathbf{r})$ contains 16 terms, but is not as constructive as $\mathbf{S}_{3\times2}(\mathbf{r})$, as shown in Section III-B. Numerical exploration reveals that the configuration, as shown in Fig. 4(b), yields a perfect condition number of 1 when the length scale l is set to 1.

The system in this configuration requires six sets of sensor modules positioned on both sides of three principal axes with equal distances, and this increases the complexity of the space layout as well as both electronic and mechanical designs. In addition, the possible orientation installation error of these one-axis accelerometers most likely counteracts the advantage of the perfect structure matrix inversion, thus keeping noise levels the same. Therefore, in the following sections, we focus on the analysis of the system with three two-axis accelerometers, as described in Section III-B, which requires half sets of sensor modules comparing to the current arrangement.

IV. Analysis of Sensor Position and Orientation Errors

Equation (1) or (13) reveals that the performance of the state derivation depends not only on the sensor readings, but also on the position and the orientation of the sensors. Therefore, an analysis of the sensor installation error is discussed in this section.

A. Nominal Condition

Equation (8) reveals that the desired angular velocity state is solely determined by the readings from gyros, and (13) reveals that the desired linear and angular acceleration states are determined by both accelerometer and gyro readings as well as the positions of accelerometers. Assuming that $\mathbf{S}_{3\times2}(\mathbf{r})$ shown in (14b) and $\mathbf{W}(\mathbf{r})$ shown in (10) with the best configuration, as depicted in Fig. 4(a), are denoted as $\mathbf{S}_{3\times2}(\mathbf{r}_{\rm best})$ and $\mathbf{W}(\mathbf{r}_{\rm best})$, the quantitative relation between the acceleration outputs and the sensor inputs of the nine-axis IMU is

$$\mathbf{x}_{\rm var} = \mathbf{S}_{3\times2}(\mathbf{r}_{\rm best})^{-1}(\mathbf{a}_{\mathbf{m}} - \mathbf{W}(\mathbf{r}_{\rm best})\boldsymbol{\omega}_6(\boldsymbol{\omega}_{\mathbf{m}}))$$

$$\begin{bmatrix} a_x \\ a_y \\ a_z \\ \dot{\omega}_x \\ \dot{\omega}_y \\ \dot{\omega}_z \end{bmatrix} = \begin{bmatrix} m & 0 & 0 & m & 0 & 0 \\ 0 & m & 0 & 0 & m & 0 \\ 0 & 0 & m & 0 & 0 & m \\ n & n & n & -n & -n & -n \\ -n & -n & n & n & n & -n \\ n & -n & n & -n & n & -n \end{bmatrix} \begin{bmatrix} a_1 \\ a_2 \\ a_3 \\ a_4 \\ a_5 \\ a_6 \end{bmatrix}$$

$$- \begin{bmatrix} 0 & 0 & 1 & 0 & 0 & 0 \\ 0 & 1 & 0 & 0 & 0 & 0 \\ -1 & 0 & 0 & 0 & 0 & 0 \\ 0 & 0 & 0 & -1 & -1 & 0 \\ 0 & 0 & 0 & 1 & 0 & 1 \\ 0 & 0 & 0 & 0 & -1 & 1 \end{bmatrix} \begin{bmatrix} \omega_1^2 + \omega_2^2 \\ \omega_1^2 + \omega_3^2 \\ \omega_2^2 + \omega_3^2 \\ \omega_1\omega_2 \\ \omega_1\omega_3 \\ \omega_2\omega_3 \end{bmatrix} \quad (16)$$

where $m = 0.5$ and $n = 0.25$. Since the optimal configuration is symmetric with respect to the three principal axes, similar composition of the three components of the state is expected, and (16) confirms this expectation. The difference in sign results from the position of these three sensory suites relative to the three principal axes and the assignments of sensing directions that are all toward positive directions of the principal axes, as shown in Fig. 4(a).

The sensing directions of the accelerometers $\{\, a_1 \quad a_4 \,\}$, $\{\, a_2 \quad a_5 \,\}$, and $\{\, a_3 \quad a_6 \,\}$ are toward the x, y, and z principal axes of the body frame, respectively. Equation (16) shows that in addition to gyro's effect, the linear acceleration $a_{i,\, i=x,y,z}$, is only affected by the accelerometers measuring in the same direction, and these two readings affect the measurement of a_i equally with scaling factor $m = 0.5$, like the "average" process. On the other hand, (16) shows that the angular acceleration $\dot{\boldsymbol{\omega}}_{i,i=x,y,z}$ is affected by all accelerometer measurements, and the effect of each individual accelerometer to $\dot{\boldsymbol{\omega}}_i$ is down to a quarter, $n = 0.25$. Interestingly, the derivation of the angular acceleration from accelerometer measurements shown in (16) is in some sense like a differential process, which means that two accelerometer measurements in the same sensing direction will be multiplied by constants with the same magnitude but with different signs before addition. For example, in the derivation of $\dot{\boldsymbol{\omega}}_x$, the first three measurements $a_{j,\, j=1,2,3}$, are multiplied by n, but the other three measurements $a_{j,\, j=4,5,6}$, are multiplied by $-n$. This is true for $\dot{\boldsymbol{\omega}}_i$ in all three directions. Because the accelerometers with the same sensing direction are affected by the same amount of gravity-induced acceleration, the differential process indeed cancels the gravity-induced portions no matter what the reading is. Therefore, the derivation of the angular acceleration in the proposed system is indeed free of gravity effect. The system yields the correct angular acceleration even if the accelerometers do not go through the gravity compensation process.

Equation (17) shown next describes the detailed relation between accelerometer readings and body state under the current optimized configuration

$$\mathbf{a}_{\mathbf{m}} = \mathbf{S}_{3\times2}(\mathbf{r}_{\rm best})[\, \mathbf{a}_{\rm COM}^T \quad \dot{\boldsymbol{\omega}}^T]^T + \mathbf{W}(\mathbf{r}_{\rm best})\boldsymbol{\omega}_6(\boldsymbol{\omega}). \quad (17)$$

If the measurements from accelerometers and gyros are correct, it is clear that the $\mathbf{x}_{\rm var}$ yields the desired acceleration states by inserting (17) into (16).

B. Sensor With Position Error

In practical implementation, unperfected installation might induce sensor positioning error. A rigid moving body has uniform angular velocity, so positioning of the gyro is not crucial. On the other hand, (1) shows that the positions of the accelerometers affect the sensor readings unless the moving body lacks rotational motion (i.e., $\boldsymbol{\omega}$ and $\dot{\boldsymbol{\omega}}$ are both zero). Thus, an analysis of accelerometer positioning is performed in this section.

The general percentage error equation utilized in this and the following sections is

$$E(X,\Delta)=\frac{|X-X^*|}{|X^*|} \tag{18}$$

where Δ denotes the error of a specific parameter and X and X^* denote the state of interest and its nominal value, respectively.

The analysis of the traditional IMU as the basis for comparison is detailed as follows. The position vector from the COM to the traditional IMU is denoted as $\mathbf{r}_0$, and its reading is denoted as $\mathbf{a}_0$. If the sensor is installed precisely at the COM as planned, $\mathbf{r}_0$ is a zero vector and $\mathbf{a}_0$ is equal to $\mathbf{a}_{\rm COM}$, as shown in (1) and (2a). If the sensor is installed with Δr_{0x} error, the angular acceleration and velocity of the body also affect the readings of $\mathbf{a}_0$ due to the Newton dynamics shown in (1). In this case, the percentage errors are

$$\begin{aligned}
E(a_x,\Delta r_{0x})&=\frac{\left|-(\omega_y^2+\omega_z^2)\Delta r_{0x}\right|}{|a_x|}\\
E(a_y,\Delta r_{0x})&=\frac{|(\dot\omega_z+\omega_x\omega_y)\Delta r_{0x}|}{|a_y|}\\
E(a_z,\Delta r_{0x})&=\frac{|(-\dot\omega_y+\omega_x\omega_z)\Delta r_{0x}|}{|a_z|}
\end{aligned} \tag{19}$$

which suggests that the percentage error is strongly determined by the relative magnitudes among the states in (1). Because of geometrical symmetry among the three principal axes, the analysis of Δr_{0y} and Δr_{0z} is neglected due to the similarity in their structures as that of Δr_{0x} shown in (19). For example, the structure of $E(a_y,\Delta r_{0y})$ is similar to that of $E(a_x,\Delta r_{0x})$.

The positioning error analysis of the nine-axis system is detailed as follows. Assuming that $\mathbf{S}_{3\times2}(\mathbf{r}_{\rm best},\Delta r_{jk})_{j=1,3,5;\,k=x,y,z}$ and $\mathbf{W}(\mathbf{r}_{\rm best},\Delta r_{jk})$denote the existence of one position error Δr_{jk} in $\mathbf{S}_{3\times2}(\mathbf{r}_{\rm best})$and $\mathbf{W}(\mathbf{r}_{\rm best})$,respectively, and the sensors are correctly installed without any orientation error, the corresponding accelerometer readings according to (17) become

$$\begin{aligned}
\mathbf{a_m}(\Delta r_{jk})=\mathbf{S}_{3\times2}(\mathbf{r}_{\rm best},\Delta r_{jk})[\,\mathbf{a}_{\rm COM}^T\quad\dot{\boldsymbol\omega}^T]^T\\
+\mathbf{W}(\mathbf{r}_{\rm best},\Delta r_{jk})\boldsymbol\omega_6(\boldsymbol\omega).
\end{aligned} \tag{20}$$

Thus, by importing (20) into (13), the acceleration states are

$$\begin{aligned}
\mathbf{x}_{\rm var}(\Delta r_{jk})&=\mathbf{S}_{3\times2}(\mathbf{r}_{\rm best})^{-1}(\mathbf{a_m}(\Delta r_{jk})-\mathbf{W}(\mathbf{r}_{\rm best})\boldsymbol\omega_6(\boldsymbol\omega_{\mathbf{m}}))\\
&=\mathbf{S}_{3\times2}(\mathbf{r}_{\rm best})^{-1}\mathbf{S}_{3\times2}(\mathbf{r}_{\rm best},\Delta r_{jk})[\,\mathbf{a}_{\rm COM}^T\quad\dot{\boldsymbol\omega}^T]^T\\
&\quad+\mathbf{S}_{3\times2}(\mathbf{r}_{\rm best})^{-1}(\mathbf{W}(\mathbf{r}_{\rm best},\Delta r_{jk})\\
&\quad-\mathbf{W}(\mathbf{r}_{\rm best}))\boldsymbol\omega_6(\boldsymbol\omega)
\end{aligned} \tag{21}$$

where $\boldsymbol\omega_{\mathbf{m}}$ is replaced by $\boldsymbol\omega$ based on (8). If the sensor is installed with position error Δr_{1x}, the corresponding error equations are

$$\begin{aligned}
E(a_x,\Delta r_{1x})&=\frac{\left|-(\omega_y^2+\omega_z^2)\Delta r_{0x}\right|}{2\,|a_x|}\\
E(a_y,\Delta r_{1x})&=\frac{|(\dot\omega_z+\omega_x\omega_y)\Delta r_{0x}|}{2\,|a_y|}\\
E(a_z,\Delta r_{1x})&=0
\end{aligned}$$

$$\begin{aligned}
E(\dot\omega_x,\Delta r_{1x})&=\frac{\left|(\dot\omega_z+\omega_x\omega_y-\omega_y^2-\omega_z^2)\Delta r_{1x}\right|}{4\,|\dot\omega_x|}\\
E(\dot\omega_y,\Delta r_{1x})&=\frac{\left|(-\dot\omega_z-\omega_x\omega_y+\omega_y^2+\omega_z^2)\Delta r_{1x}\right|}{4\,|\dot\omega_y|}\\
E(\dot\omega_z,\Delta r_{1x})&=\frac{\left|(-\dot\omega_z-\omega_x\omega_y-\omega_y^2-\omega_z^2)\Delta r_{1x}\right|}{4\,|\dot\omega_z|}.
\end{aligned} \tag{22}$$

It is obvious that the percentage errors of a_x and a_y states of the nine-axis system shown in (22) are half that of the traditional IMU shown in (19), which matches the intuition that two acceleration measurements are taken in the nine-axis system, so the effect of the positioning error of the individual sensor is reduced by half. Unlike the error Δr_{0x} in the traditional IMU affecting all three states shown in (19), the performance of the third linear acceleration state a_z is not affected by the variation Δr_{1x} because the accelerometer readings affected by Δr_{1x} are $\{\,a_1\quad a_2\,\}$, and these two readings do not contribute to the state a_z shown in (16). On the other hand, $\{\,a_1\quad a_2\,\}$ affects all three components of angular acceleration shown in (16); thus, the position error Δr_{1x} appears in all three components.As shown in Fig. 4(a), the components of the nominal value of position vectors are "normalized" to 1 in the optimal configuration; thus, the magnitude of Δr_{1x} directly represents the amount of error. For example, $\Delta r_{1x}=0.1$ equals a 10% error in r_{1x} component. Thus, the quantitative analysis can be derived if the motion states are known.

C. Sensor With Orientation Error

In practical implementation, both the accelerometers and the gyros might have orientational installation errors. As mentioned in Section II, the directions of the sensors are generally set to align with the principal axes since the body motion is represented in this coordinate. If orientations of the three one-axis sensors do not align with the principal axes, but are linearly independent, a linear relation exists between the raw sensor data and the desired sensory information in the body coordinate

$$\mathbf{s_m}=\mathbf{Rs}=\begin{bmatrix}R_{11}&r_{12}&r_{13}\\r_{21}&R_{22}&r_{23}\\r_{31}&r_{32}&R_{33}\end{bmatrix}\mathbf{s} \tag{23}$$

where $\mathbf{s_m}$ is the measurement vector with three linear-independent components, $\mathbf{s}$ is the state vector along with three principal axes, and $\mathbf{R}$ is a 3×3 matrix. If the sensors are oriented precisely to the principal axes, the operator $\mathbf{R}$ is merely an identity matrix (i.e., the ideal case $R_{i\,i}=1$, $r_{i\,j}=0$, $_{i,\,j=1,2,3,i\neq j}$). The linear operator $\mathbf{R}$ is a rotation matrix if three sensing directions are mutually orthogonal, which is reasonably held for commercial multiaxis inertial sensors. The numerical analysis shows that if the orientation error is 2° with respect to the $[\,1\quad1\quad1\,]$ rotating axis and assuming the same amount of errors in all three axes represented as $E_R([\,1\quad1\quad1\,],2^\circ)$, the diagonal terms of the $\mathbf{R}$, $R_{i\,i},i=1,2,3$, are $\sim$0.9996 and the off-diagonal terms of the $\mathbf{R}$, $r_{i\,j,i\neq j}$, are $\sim$0.02. This reveals that the motion supposedly to be measured by a certain sensor has 0.04% measurement error, and it indicates a 2% crosstalk error. For the 5° case, the former is 0.25% and the latter is 5%.

According to (23), if the gyro has an orientational error, the relation between the three-axis measurement data and the angular velocity state represented in the body coordinate is no longer equal to (8), but in the form

$$\boldsymbol{\omega}_{\mathbf{m}} = \mathbf{R}_{\boldsymbol{\omega}}\boldsymbol{\omega}. \tag{24}$$

For both the traditional and the proposed IMUs, since the angular velocity state measured by the gyros is already the desired state, the state measurement error caused by orientational installation error is determined by $\mathbf{R}_{\boldsymbol{\omega}}$ only. The accelerometers have no effect on this state.

Likewise, if the accelerometers of the traditional IMU have an orientational error, a relation similar to (23) exists

$$\mathbf{a}_{\mathbf{m}} = \mathbf{R}_{\mathbf{T}}\,\mathbf{a}_{\mathrm{COM}}. \tag{25}$$

The associated error equation can then be derived as follows:

$$E(a_x, \mathbf{R}_{\mathbf{T}}) = \frac{|(R_{11}-1)a_x + r_{21}a_y + r_{31}a_z|}{|a_x|} \tag{26}$$

where R_{11} and $r_{i1,i=1,2,3}$, are diagonal and off-diagonal terms of the operator $\mathbf{R}_T$.

The linear and angular acceleration states of the proposed nine-axis system are derived according to the linear operation shown in (16). How the orientation error affects the acceleration measurement $\mathbf{x}_{\mathrm{var}}$ requires further analysis. In the first scenario, assuming that the accelerometers are oriented correctly, but the gyros are not, the desired acceleration state $\mathbf{x}_{\mathrm{var}}$ can be obtained by importing (24) and (17) into (16)

$$\begin{aligned}\mathbf{x}_{\mathrm{var}}(\mathbf{R}_{\boldsymbol{\omega}}) = {} & [\,\mathbf{a}_{\mathrm{COM}}^{T} \quad \dot{\boldsymbol{\omega}}^{\,T}]^{T} \\ & + \mathbf{S}_{3\times 2}(\mathbf{r}_{\mathrm{best}})^{-1}\mathbf{W}(\mathbf{r}_{\mathrm{best}})(\boldsymbol{\omega}_6(\boldsymbol{\omega}) - \boldsymbol{\omega}_6(\mathbf{R}_{\boldsymbol{\omega}}\boldsymbol{\omega})).\end{aligned} \tag{27}$$

Each state in the expanded form of (25) has several terms due to the coupling effect of the sensor readings among all three spatial principal axes. The corresponding error equations are

$$E(a_x, \mathbf{R}_{\boldsymbol{\omega}}) = \frac{\left|\begin{array}{l} -(r_{21}^2 + r_{31}^2)\omega_x^2 + (1 - R_{22}^2 - r_{32}^2)\omega_y^2 \\ \quad +(1 - R_{33}^2 - r_{23}^2)\omega_z^2 - 2(R_{22}r_{21} + r_{31}r_{32})\omega_x\omega_y \\ \quad -2(R_{33}r_{31} + r_{21}r_{23})\omega_x\omega_z - 2(R_{22}r_{23} + R_{33}r_{32})\omega_y\omega_z \end{array}\right|}{|a_x|}$$

$$E(\dot{\omega}_z, \mathbf{R}_{\boldsymbol{\omega}}) = \frac{\left|\begin{array}{l} R_{11}(r_{21} + r_{31})\omega_x^2 + r_{12}(R_{22} + r_{32})\omega_y^2 \\ \quad +r_{13}(R_{33} + r_{23})\omega_z^2 \\ \quad +(R_{11}R_{22} - 1 + R_{11}r_{32} + r_{12}r_{21} + r_{12}r_{31})\omega_x\omega_y \\ \quad +(R_{11}R_{33} - 1 + R_{11}r_{23} + r_{13}r_{21} + r_{13}r_{31})\omega_x\omega_z \\ \quad +(R_{22}r_{13} + R_{33}r_{12} - r_{12}r_{23} - r_{13}r_{32})\omega_y\omega_z \end{array}\right|}{|\dot{\omega}_z|} \tag{28}$$

where $R_{i\,i,i=1,2,3}$, and $r_{i\,j,i\neq j}$, are diagonal and off-diagonal terms of the operator $\mathbf{R}_{\boldsymbol{\omega}}$. The error equations of the other four states are skipped due to the similarity in structure as the two shown in (28). Since the angular velocity state affects the acceleration readings through the double cross-product term shown in (4), its effect to (28) appeared in quadratic forms. The coefficients in (28) are composed by the summation of the multiplications of the differently selected two terms of $\mathbf{R}_{\boldsymbol{\omega}}$. Because of the multiplications, the effect of each term is further reduced. For example, the coefficients of the six-term quadratic representation of angular velocity in $E(a_x, \mathbf{R}_{\boldsymbol{\omega}})$with $E_R([\,1 \quad 1 \quad 1\,], 2^\circ)$ are -0.0008, 0.0004, 0.0004, -0.0400, 0.0406, and -0.0010, respectively. These in $E(\dot{\omega}_x, \mathbf{R}_{\boldsymbol{\omega}})$ are 0.0005, -0.0203, 0.0200, 0.0196, -0.0207, and 0.0013, respectively. Therefore, in general, the effects are small, and the quantitative error analysis can be derived if the motion states are known.

In the second scenario, assume that the accelerometer at position I has orientation error $\mathbf{R}_{\mathbf{I}}$ and the remaining accelerometers and gyros are oriented correctly. By assigning the acceleration along with the third measurement axis at position I as $\tilde{a}_7$, the measured acceleration can be derived by combining (1) and (23)

$$[\,\tilde{a}_1 \quad \tilde{a}_2 \quad \tilde{a}_7\,]^T = \mathbf{R}_{\mathbf{I}}(\mathbf{a}_{\mathrm{COM}} + \dot{\boldsymbol{\omega}} \times \mathbf{r}_1 + \boldsymbol{\omega} \times (\boldsymbol{\omega} \times \mathbf{r}_1)) \tag{29}$$

where the first two components on the left side are new measurements data affected by the orientational error. Instead of (5a), the revised accelerometer measurement array is

$$\mathbf{a}_{\mathbf{m}}(\mathbf{R}_{\mathrm{I}}) = [\,\tilde{a}_1 \quad \tilde{a}_2 \quad a_3 \quad a_4 \quad a_5 \quad a_6\,]^T \tag{30}$$

and the acceleration state can be obtained by

$$\mathbf{x}_{\mathrm{var}}(\mathbf{R}_{\mathbf{I}}) = \mathbf{S}_{3\times 2}(\mathbf{r}_{\mathrm{best}})^{-1}(\mathbf{a}_m(\mathbf{R}_{\mathbf{I}}) - \mathbf{W}(\mathbf{r}_{\mathrm{best}})\boldsymbol{\omega}_6(\boldsymbol{\omega}_m)). \tag{31}$$

Similar to (27), each state in the expanded form of (31) has several terms due to the coupling effect of the sensor readings among all three spatial principal axes. The corresponding error equations are

$$E(a_x, \mathbf{R}_{\mathbf{I}}) = \frac{\left|\begin{array}{l} (R_{11}-1)a_x + r_{21}a_y + r_{31}a_z + (r_{21} - r_{31})\dot{\omega}_x \\ \quad +(1 - R_{11} + r_{31})\dot{\omega}_y + (R_{11} - 1 - r_{21})\dot{\omega}_z \\ \quad +r_{31}\omega_x^2 + r_{21}\omega_y^2 + (R_{11} - 1)\omega_z^2 \\ \quad +(1 - R_{11} - r_{21})\omega_x\omega_y + (1 - R_{11} - r_{31})\omega_x\omega_z \\ \quad -(r_{21} + r_{31})\omega_y\omega_z \end{array}\right|}{2\,|a_x|}$$

$$E(\dot{\omega}_z, \mathbf{R}_{\mathbf{I}}) = \frac{\left|\begin{array}{l} (R_{11} - 1 + r_{12})a_x + (R_{22} - 1 + r_{21})a_y \\ \quad +(r_{31} + r_{32})a_z \\ \quad +(R_{22} - 1 + r_{21} - r_{31} - r_{32})\dot{\omega}_x \\ \quad +(1 - R_{11} - r_{12} + r_{31} + r_{32})\dot{\omega}_y \\ \quad +(R_{11} - R_{22} + r_{12} - r_{21})\dot{\omega}_z \\ \quad +(r_{31} + r_{32})\omega_x^2 \\ \quad +(R_{22} - 1 + r_{21})\omega_y^2 + (R_{11} - 1 + r_{12})\omega_z^2 \\ \quad +(2 - R_{11} - R_{22} - r_{12} - r_{21})\omega_x\omega_y \\ \quad +(1 - R_{11} - r_{12} - r_{31} - r_{32})\omega_x\omega_z \\ \quad +(1 - R_{22} - r_{21} - r_{31} - r_{32})\omega_y\omega_z \end{array}\right|}{4\,|\dot{\omega}_z|} \tag{32}$$

where $R_{i\,i,i=1,2,3}$, and $r_{i\,j,i\neq j}$, are diagonal and off-diagonal terms of the operator $\mathbf{R}_{\mathbf{I}}$. As in the case with a gyro orientation error, the error equations of the other four states are skipped due to the similarity in structure as the two shown in (32). Unlike the case in which the gyros have orientation errors, the orientation errors of the accelerometers have a more complicate effect on the acceleration measurement. According to (1), the acceleration readings at any point except the origin are determined by the linear and angular acceleration as well as the angular velocity.

Thus, once the orientational error of the accelerometer exists, all states appear in the error equation, as shown in (32). In the case of orientational error $\mathbf{R_I}$ equal to $E_R([1 \quad 1 \quad 1], 2^\circ)$, the coefficients of the 12-term state in $E(a_x, \mathbf{R_I})$ are -0.0002, 0.0102, -0.0100, 0.0202, -0.0098, -0.0104, -0.0100, 0.0102, -0.0002, -0.0100, 0.0102, and -0.0003. Those in $E(\dot{\omega}_z, \mathbf{R_I})$ are -0.0051, 0.005, 0.0001, 0.0049, 0.0052, -0.0101, 0.0001, 0.0050, -0.0051, 0.0001, 0.0050, and -0.0051. Therefore, in general, the effects are small, and the quantitative error analysis can be derived if the motion states are known.

D. Short Discussion

The body states of a rigid body during spatial motion always follow certain rules based on the Newton mechanics, as shown in (1), which basically defines the relations among the linear accelerations of arbitrary points on the body, angular acceleration, and angular velocity of the body. Therefore, these states appear in the error equations, while certain installation errors exist. Though the position error of the accelerometer "shifts" the acceleration measurement to another point, fewer terms of the angular acceleration and velocity appear in the error equations shown in (22) than in the case of orientation errors shown in (28) and (32) because the latter case induces the coupling effects among all three axes. No matter in the traditional IMU or in the nine-axis system, the quantitative measures of the errors require the information of the actual body states.

For traditional and nine-axis IMUs, the angular velocity state is directly measured by the gyros; thus, this measurement is affected only by the orientation of the gyros and not by their positions or the status of the accelerometers. As for the linear acceleration state, the traditional IMU measures this state by accelerometers only. Consequently, fewer states appear in the error equations shown in (19) and (26). The nine-axis system requires data from the accelerometers and the gyros to compute this state, so more terms are involved in the error equations shown in (22), (28), and (32). This is the tradeoff of not having measurements directly at the desired location (i.e., at COM). However, because of this arrangement, the allocations of the sensors have more flexibility, and the effects of errors in the individual sensors are reduced. More specifically, by comparing (19) and (22) as well as (26) and (32), the numbers 2 and 4 are at the denominators in (22) and (32). In addition, the angular acceleration state can be derived from instant data—a memoryless process, and its measurement error due to installation errors can be quantified as the linear combinations of the body states. In the traditional IMU, the angular acceleration state is derived by the differentiation of the angular velocity state. Thus, a sequence of data with a high sampling rate is required, and the quantitative error amount is determined not only by $\mathbf{R}_\omega$, but also by the subsequently differentiation and filtering processes that may vary significantly among the techniques adopted.

If the traditional IMU is not installed at COM [assuming at $\mathbf{a}_p$ shown in (1)], the derivation of the angular velocity measured by the gyros remains intact. However, the recovery of COM linear acceleration $\mathbf{a}_o$ now depends on not only the values associated with the accelerometer $\mathbf{a}_p$ and $\mathbf{r}_p$, but also the readings of angular acceleration and velocity based on the Newton mechanics shown in (1). This implies that the signal quality of the COM linear acceleration now hinges on that of the differentiated angular acceleration.

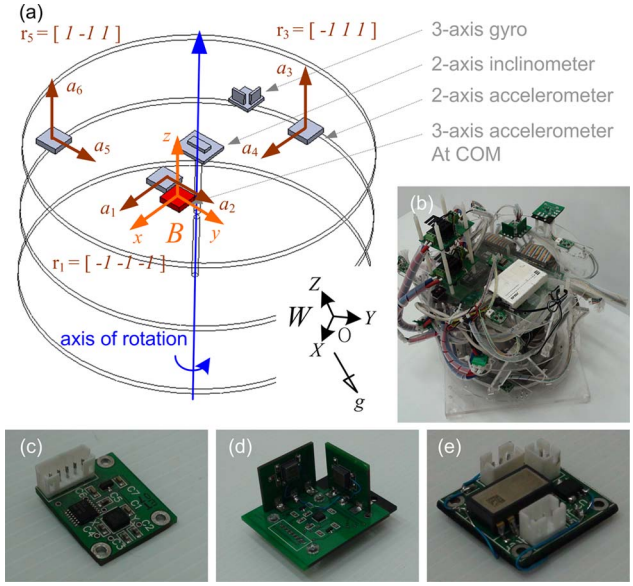

Fig. 5. Experimental apparatus. (a) Sketch of the nine-axis IMU. (b) Image of the apparatus. (c)–(e) Images of the three-axis accelerometer module, six-axis IMU module, and two-axis inclinometer module, respectively. The apparatus is tilted during experiments, so the accelerometer measurements are affected by both apparatus motion and gravity effect in a time-variant manner.

V. Experimental Evaluation

The benchtop apparatus with one controllable rotational DOF, as shown in Fig. 5(a)–(b), was utilized for experimental evaluation of the proposed nine-axis system. The required sensory measurements were obtained from three three-axis accelerometers (ADXL330, ± 3 g, Analog Device, using two-axis only), three one-axis gyros (ADXRS610, $\pm 300^0$ per second, Analog Device), and one two-axis inclinometer (SCA100 T, $\pm 90^0$, VTI Technologies). The photographs of these custom-made modules are shown in Fig. 5(c)–(e). In addition, a three-axis accelerometer (ADXL330) was also mounted at the "virtual" COM for performance comparison (as the "traditional IMU"). The accelerometers of the nine-axis system are mounted according to the best configuration, as shown in Fig. 4(a), with $l = 100$ mm. In the numerical computations, the length unit was changed to decimeter ($l = 1$), as suggested in Section III.B, and the final results were presented in standard SI MKS units. A real-time embedded control system (sbRIO-9632, National Instruments) running at 500 Hz was in charge of sensor signal collection and position-controlled rotating motion generation. All of the 32 analog input channels of the sbRIO have ± 10 V range and 16-bit A–D resolutions. By considering mechanical structure manufacturing and printed circuit board (PCB) positioning, the sensor positioning accuracy can be controlled within 1 mm. Thus, for the apparatus with $l = 100$ mm utilized in this paper, $\Delta r = 0.01$ equals to 1%. Together with the projected range of the states, the effect of the error to the state derivation can be roughly estimated by (19) and (22).

TABLE I
RMS NOISE OF THE SENSORS AND THE MECHATRONIC SYSTEM

	Accelerometer (m/s^2)		
	a_x	a_y	a_z
Sensor	0.0776	0.0776	0.0970
System	0.0823	0.0831	0.1078
	Gyroscope ($^0/s$)		
	ω_x	ω_y	ω_z
Sensor	0.4472	0.4472	0.4472
System	0.5416	0.5597	0.5667

TABLE II
COMPARISON OF THE RMS NOISES OF THE TRADITIONAL IMU AND NINE-AXIS SYSTEMS

	Linear acceleration (m/s^2)			Angular acceleration (rad/s^2)		
	a_x	a_y	a_z	$\dot{\omega}_x$	$\dot{\omega}_y$	$\dot{\omega}_z$
Traditional	0.0874	0.0812	0.1108	5.9104	6.3150	6.1903
9-axis	0.0514	0.0672	0.0754	0.5661	0.4921	0.6023

Table I lists the rms noises of the sensors themselves and of the mechatronic systems. They are the means of several datasets. The sensor noises are derived from the noise density provided in the datasheet [30], [31], with the integration of the spectrum with the approximated one-pole system model. The system noises are empirically measured, while the apparatus is stationary. This data represent the signal quality of the whole mechatronic system. For both sensors, Table I shows that the rms noise of the overall system is similar to that of the sensors themselves, which confirms that the acquisition setup is functional.

Table II compares the rms noises of the traditional IMU to the proposed nine-axis system. They are the means of several datasets as well. The left three columns list the COM linear acceleration; the noise data of traditional IMU are acquired directly from the three-axis module mounted at the COM; thus, they are identical to the data, as shown in Table I. The noise data of the nine-axis system are derived from (16) with accelerometer and gyro measurements, and they show that redundancy of the sensors improves the signal quality. The right three columns in Table II reveal that the noise of angular acceleration derived by (13) in the nine-axis system is much better than that from traditional IMU, which, in general, uses differentiation of gyro signals.

The proposed nine-axis system was evaluated by two different testing setups: the swing test on a benchtop apparatus with its frame fixed to the world frame and the other is a free arbitrary motion test. The details are described in the following two sections.

A. Swing Test

In this setup, the benchtop apparatus was rigidly fixed to the world frame, and the "virtual" COM of the proposed nine-axis system was positioned on the rotating apparatus at a designated distance 30 mm to the rotational axis along the minus y-axis of the body frame B, not at the axis [see Fig. 5(a)]. Thus, the COM could be subjected to linear and angular accelerations while the apparatus rotated. Empirically, it rotated in a sinusoidal motion

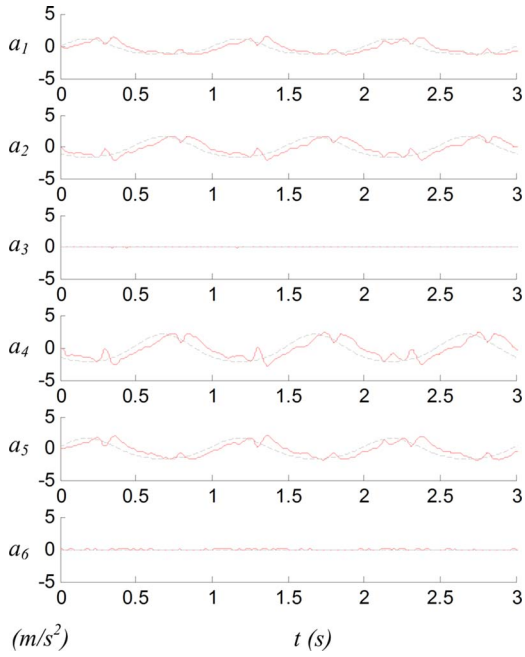

Fig. 6. Ideal (gray dashed line) and measured (red solid line) accelerations of a_1–a_6 at three sensor positions while the apparatus is subjected to sinusoidal swing motion.

with amplitude of 23.5° and frequency of 1 Hz, so theoretically, the COM was subjected to sinusoidal tangent, normal, and angular accelerations. In addition, the ideal accelerations at all sensor positions, a_1 to a_6, can be calculated according to (1), as shown in the gray dashed lines in Fig. 6. Because of the offset and the double cross-product term, the ideal accelerations at these locations were the compositions of several sinusoidal functions, unlike the simple single sinusoidal motion shown at the COM. Since a_3 and a_6 measure the accelerations parallel to the rotation axis, the readings induced by motion are supposed to be zeros.

To make the testing scenario more realistic to practical applications, the rotating axis of the turntable was tilted 12° from the vertical axis, so the gravity-induced acceleration affected all accelerometer readings in a time-variant manner while the table rotated. The gravity compensation was in accordance with the known orientation provided by the encoder on the apparatus. That procedure was executed before the sensor readings were imported into (16). The measured accelerations, as shown in Fig. 6 (red solid lines), are after gravity compensation.

Fig. 7(a) plots the theoretical estimated and experimental measured body states while the apparatus was operated in the sinusoidal motion. To make the plots presentable, states are processed with a Chebyshev filter. The associated statistical data are listed in Table III, where the rms errors data are compared with theoretical estimated states. Due to 1 DOF rotation of the benchtop apparatus, the effective linear accelerations are 2-D, spanned in the plane perpendicular to the rotational axis, as shown in Fig. 5(a) (i.e., the xy plane in the body frame). The effective angular acceleration and velocity are both 1-D along with the rotation axis (i.e., $\dot{\omega}_z$ and ω_z). Thus, other states, as shown in Table III, can be treated as operation noises, including a_z, ω_x, ω_y, $\dot{\omega}_x$, and $\dot{\omega}_y$. In addition, the linear acceleration

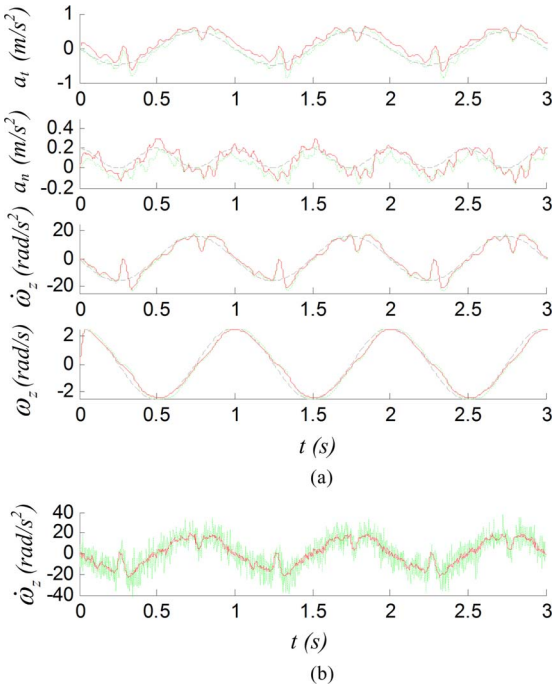

Fig. 7. (a) Comparison of states obtained from different methods after filtering. Subplots from top to bottom are tangential acceleration a_t, normal acceleration a_n, angular acceleration $\dot{\omega}_z$, and angular velocity ω_z, respectively. Notations: gray dashed line: ideal curve derived from desired position control trajectories; green dotted line: state derived from traditional IMU; red solid line: state derived from nine-axis system. Experimental data are processed with gravity compensation. (b) Comparison of raw angular acceleration data from the traditional IMU (green dotted line) and the nine-axis system (red solid line).

TABLE III
COMPARISON OF THE RMS ERROR OF THE TRADITIONAL IMU AND THE NINE-AXIS SYSTEM TO THE THEORETICAL ESTIMATED STATES WHILE THE APPARATUS ROTATED IN THE SINUSOIDAL MOTION

	Linear acceleration (m/s^2)			Angular acceleration (rad/s^2)		
	a_t	a_n	a_z	$\dot{\omega}_x$	$\dot{\omega}_y$	$\dot{\omega}_z$
Traditional	0.1383	0.0614	0.0434	0.3248	0.2991	4.2943
9-axis	0.1929	0.0814	0.0275	0.4684	0.3777	4.1003
	Angular velocity (rad/s)					
	ω_x	ω_y	ω_z			
Traditional 9-axis	0.0186	0.0148	0.3638			

states are represented in tangential and normal accelerations a_t and a_n because of their better physical implications than those represented in the Cartesian body coordinates. The first and second subplots of Fig. 7(a) show that even though the sensors of the proposed nine-axis system (red solid lines) are not located at the COM, they can be utilized to recover the COM linear acceleration by comparing the curves to the theoretical ones (gray dashed lines) and those measured by the traditional IMU located at the COM (green dotted lines). Though the experimental curves show vibrating behavior because of the imperfect position-based motion control and empirically unrigid apparatus structure, the trends of the curves, in general, match each other. The third subplot shows that the angular acceleration state can also be correctly derived by the nine-axis system that closely

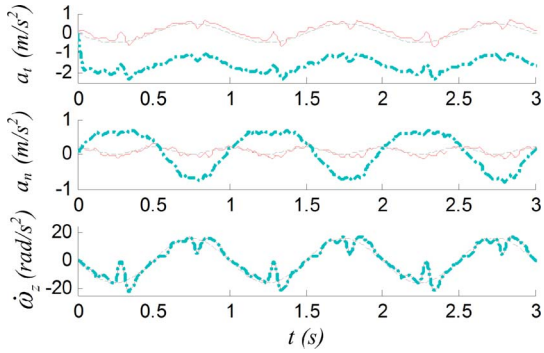

Fig. 8. Comparison of the states obtained from theoretically estimated (gray dashed line) and empirically measured by the nine-axis system with (red solid line) and without (blue thick-dash dotted line) gravity compensation.

TABLE IV
RMS ERROR BETWEEN THE TRADITIONAL IMU AND THE NINE-AXIS SYSTEM WHILE THE APPARATUS MOVED ARBITRARILY IN THE SPATIAL SPACE

Linear acceleration (m/s^2)			Angular acceleration (rad/s^2)		
a_t	a_n	a_z	$\dot{\omega}_x$	$\dot{\omega}_y$	$\dot{\omega}_z$
0.1713	0.0854	0.0724	0.9331	0.7506	0.8960

matches the curve of the traditional IMU. Since traditional and proposed nine-axis systems used the same gyro to measure the angular velocity, the fourth subplot of Fig. 7(a) only contains one experimental curve and the bottom row of Table III represents the experimental data shared by both systems. The raw angular acceleration measurements without any filtering [see Fig. 7(b)] indicate that the data from the nine-axis system are much cleaner than that from the traditional IMU, and the implementation of Chebyshev filter may be skipped.

Fig. 8 compares the acceleration states derived by the nine-axis system with (red solid line) and without (blue thick dash dotted line) gravity compensation. As expected, the first two subplots show that the derivation of linear accelerations does require gravity compensation as that from the traditional IMU. On the contrary, the compensated and uncompensated angular accelerations shown in the third subplot are identical, confirming that the angular acceleration is free of a gravity effect in the nine-axis system, as described in Section IV-A.

B. Arbitrary Motion Test

In this setup, the benchtop apparatus was moved arbitrarily in the 3-D spatial space; thus, the linear and angular accelerations along all three principal axes could be induced in the test. The gravity effect was compensated by the readings of the two-axis inclinometer, and the details are briefly described in Appendix I. Table IV lists the statistical data of this experiment, where the rms errors of accelerations between measurements from the nine-axis system and the traditional IMU located at the COM are presented. Fig. 9(a) plots one typical result of the experiment. To make the plots presentable, states are processed with a Chebyshev filter as well. The top three subplots confirm that though the sensors of the proposed nine-axis system (red solid lines) are not located at the COM, they can indeed recover the COM linear acceleration. The bottom three subplots

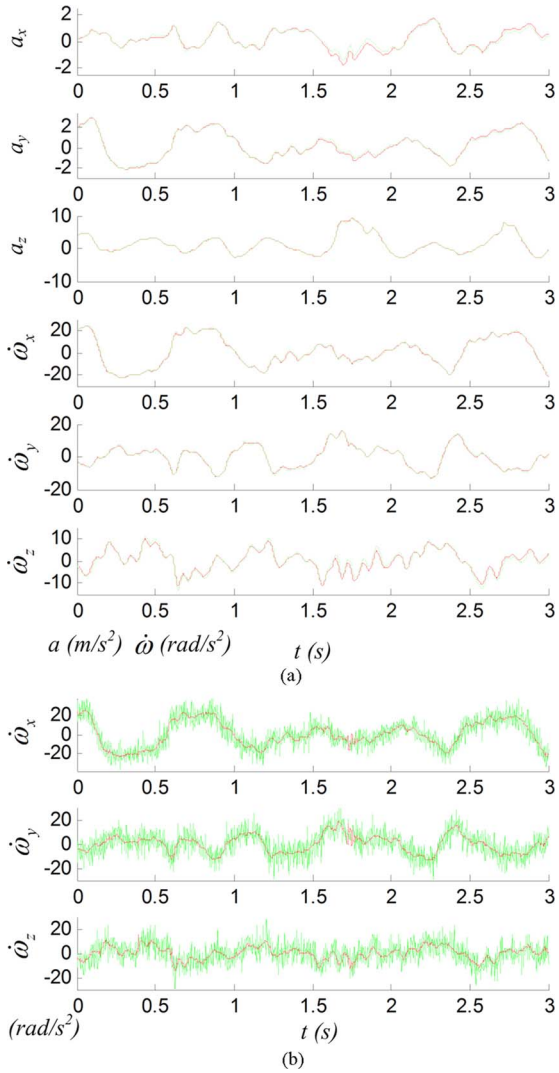

Fig. 9. (a) Comparison of the states obtained from the traditional IMU (green dotted line) and the nine-axis system (red solid line). The upper three subplots are spatial linear accelerations, and the bottom three ones are the spatial angular accelerations. Experimental data are processed with gravity compensation. (b) Comparison of raw angular acceleration data from the traditional IMU (green dotted line) and the nine-axis system (red solid line).

of Fig. 9(a) show that the angular acceleration states can be correctly derived by the nine-axis system.

The angular acceleration measurements without any filtering, as shown in Fig. 9(b), again indicate that the quality of the raw data from the nine-axis system is much better than that from the traditional IMU. Although the filtered signals in the latter case can recover the original motion states, in general, the estimated states introduce certain delay, and the system with a high sampling rate and sufficient computation power is required for filter implementation. On the contrary, the angular acceleration of the nine-axis system can be derived adequately via simple memoryless matrix computation.

VI. Conclusion

We have investigated the nine-axis IMU that utilizes a three-axis angular velocity measurement from gyros and a six-axis linear acceleration measurement from three two-axis accelerometers. The design of this sensory system was based on an analysis of rigid body dynamics and matrix theory, and an optimal configuration of the system with three two-axis accelerometers was proposed. The error analysis shows the merit of the redundancy of the sensors. The experimental results confirmed that even though the sensors of the nine-axis system are not located at the COM, the system is capable of delivering linear acceleration measurements comparable with the traditional IMU. The system also yields correct angular acceleration, and the measurement of this state is free of gravity effect as well. In addition, the computation only requires instant data, a memoryless process.

We are in the process of investigating a sensor fusion scheme of this system with other position and orientation sensors, with the intention of constructing an observable system capable of accurate full body state estimation for analysis of dynamic locomotion in legged robots.

Appendix

Gravity Compensation of Accelerometer Readings From the Measurements of a Two-Axis Inclinometer

In the empirical evaluation, a two-axis inclinometer is utilized in the arbitrary motion test, as described in Section V-B. Thus, its compensation method is briefly introduced in this section. The two-axis inclinometer mounted rigidly on the body frame measures the angles θ_x and θ_y between the gravity vector $\mathbf{g}$ and two principal axes x and y of B. The third angle θ_z can be derived based on the property of the direction cosines as follows:

$$\cos\,\theta_x^2 + \cos\,\theta_y^2 + \cos\,\theta_z^2 = 1. \tag{33}$$

Based on this relationship, the gravity vector $\mathbf{g}$ can be represented in the body frame

$${}^b\mathbf{g} = g[\,\cos\,\theta_x \quad \cos\,\theta_y \quad \cos\,\theta_z\,]^T \tag{34}$$

where $g = 9.81\ \mathrm{m/s^2}$, and three components of (34) indicate the amount of gravity-induced acceleration along the three principal axes of B. Since the sensing directions of the accelerometers are aligned with the principal axes of B as well, the gravity-compensated acceleration measurement $a_{j\,,j=1-6}$ can be derived by subtracting (34) from the raw measurement of the accelerometers.

Acknowledgment

The authors wish to express their gratitude to National Instruments' Taiwan Branch for their kind support of this study with equipment and technical consulting.

References

[1] N. Yazdi, F. Ayazi, and K. Najafi, "Micromachined inertial sensors," *Proc. IEEE*, vol. 86, no. 8, pp. 1640–1659, Aug. 1998.

[2] H. Abdellatif and B. Heimann, "Advanced model-based control of a 6-DOF hexapod robot: A case study," *IEEE/ASME Trans. Mechatronics*, vol. 15, no. 2, pp. 269–279, Apr. 2010.

[3] D. Lhomme-Desages, C. Grand, F. Ben Amar, and J. C. Guinot, "Doppler-based ground speed sensor fusion and slip control for a wheeled rover," *IEEE/ASME Trans. Mechatronics*, vol. 14, no. 4, pp. 484–492, Aug. 2009.

[4] V. Sankaranarayanan, M. E. Emekli, B. A. Guvenc, L. Guvenc, E. S. Ozturk, S. S. Ersolmaz, I. E. Eyol, and M. Sinal, "Semiactive suspension control of a light commercial vehicle," *IEEE/ASME Trans. Mechatronics*, vol. 13, no. 5, pp. 598–604, Oct. 2008.
[5] T. L. Lam, H. H. Qian, and Y. S. Xu, "Omnidirectional steering interface and control for a four-wheel independent steering vehicle," *IEEE/ASME Trans. Mechatronics*, vol. 15, no. 3, pp. 329–338, Jun. 2010.
[6] U. X. Tan, K. C. Veluvolu, W. T. Latt, C. Y. Shee, C. N. Riviere, and W. T. Ang, "Estimating displacement of periodic motion with inertial sensors," *IEEE Sensors J.*, vol. 8, no. 8, pp. 1385–1388, Aug. 2008.
[7] J. Leavitt, A. Sideris, and J. E. Bobrow, "High bandwidth tilt measurement using low-cost sensors," *IEEE/ASME Trans. Mechatronics*, vol. 11, no. 3, pp. 320–327, Jun. 2006.
[8] T. Geng and J. Q. Gan, "Planar biped walking with an equilibrium point controller and state machines," *IEEE/ASME Trans. Mechatronics*, vol. 15, no. 2, pp. 253–260, Apr. 2010.
[9] M. Ishikawa, Y. Minami, and T. Sugie, "Development and control experiment of the trident snake robot," *IEEE/ASME Trans. Mechatronics*, vol. 15, no. 1, pp. 9–16, Feb. 2010.
[10] K. S. Sollmann, M. K. Jouaneh, and D. Lavender, "Dynamic modeling of a two-axis, parallel, H-frame-type XY positioning system," *IEEE/ASME Trans. Mechatronics*, vol. 15, no. 2, pp. 280–290, Apr. 2010.
[11] R. V. Patel, H. A. Talebi, J. Jayender, and F. Shadpey, "A robust position and force control strategy for 7-DOF redundant manipulators," *IEEE/ASME Trans. Mechatronics*, vol. 14, no. 5, pp. 575–589, Oct. 2009.
[12] W. T. Ang, P. K. Khosla, and C. N. Riviere, "Nonlinear regression model of a low-g MEMS accelerometer," *IEEE Sensors J.*, vol. 7, no. 1, pp. 81–88, Jan. 2007.
[13] A. U. Alahakone and S. Senanayake, "A real-time system with assistive feedback for postural control in rehabilitation," *IEEE/ASME Trans. Mechatronics*, vol. 15, no. 2, pp. 226–233, Apr. 2010.
[14] S. K. Banala, S. K. Agrawal, S. H. Kim, and J. P. Scholz, "Novel gait adaptation and neuromotor training results using an active leg exoskeleton," *IEEE/ASME Trans. Mechatronics*, vol. 15, no. 2, pp. 216–225, Apr. 2010.
[15] J. Yoon, B. Novandy, C. H. Yoon, and K. J. Park, "A 6-DOF gait rehabilitation robot with upper and lower limb connections that allows walking velocity updates on various terrains," *IEEE/ASME Trans. Mechatronics*, vol. 15, no. 2, pp. 201–215, Apr. 2010.
[16] J. J. Crisco, J. J. Chu, and R. M. Greenwald, "An algorithm for estimating acceleration magnitude and impact location using multiple nonorthogonal single-axis accelerometers," *Trans. ASME, J. Biomech. Eng.*, vol. 126, pp. 849–854, Dec. 2004.
[17] P. Cappa, L. Masia, and F. Patane, "Numerical validation of linear accelerometer systems for the measurement of head kinematics," *Trans. ASME, J. Biomech. Eng.*, vol. 127, pp. 919–928, Nov. 2005.
[18] P. C. Lin, H. Komsuoglu, and D. E. Koditschek, "A leg configuration measurement system for full-body pose estimates in a hexapod robot (vol 21, pg 411, 2005)," *IEEE Trans. Robot.*, vol. 21, no. 3, pp. 778–778, Aug. 2005.
[19] P. C. Lin, H. Komsuoglu, and D. E. Koditschek, "Sensor data fusion for body state estimation in a hexapod robot with dynamical gaits," *IEEE Trans. Robot.*, vol. 22, no. 5, pp. 932–943, Oct. 2006.
[20] C. B. Low and D. W. Wang, "GPS-based tracking control for a car-like wheeled mobile robot with skidding and slipping," *IEEE/ASME Trans. Mechatronics*, vol. 13, no. 4, pp. 480–484, Aug. 2008.
[21] Y. C. Yang and J. A. Farrell, "Magnetometer and differential carrier phase GPS-aided INS for advanced vehicle control," *IEEE Trans. Robot. Autom.*, vol. 19, no. 2, pp. 269–282, Apr. 2003.
[22] E. Asadi and M. Bozorg, "A decentralized architecture for simultaneous localization and mapping," *IEEE/ASME Trans. Mechatronics*, vol. 14, no. 1, pp. 64–71, Feb. 2009.
[23] N. Trawny, A. I. Mourikis, S. I. Roumeliotis, A. E. Johnson, and J. F. Montgomery, "Vision-aided inertial navigation for pin-point landing using observations of mapped landmarks," *J. Field Robot.*, vol. 24, pp. 357–378, 2007.
[24] A. J. Padgaonkar, K. W. Krieger, and A. I. King, "Measurement of angular acceleration of a rigid body using linear accelerometers," *Trans. ASME, J. Basic Eng.*, vol. 42, pp. 552–556, 1975.
[25] J. H. Chen, S. C. Lee, and D. B. Debra, "Gyroscope free strapdown inertial measurement unit by 6 linear accelerometers," *J. Guid. Control Dyn.*, vol. 17, pp. 286–290, Mar./Apr. 1994.
[26] G. M. Genin and J. Genin, "Sensor placement for angular velocity determination," *Trans. ASME, J. Dyn. Syst., Meas., Control*, vol. 128, pp. 543–547, 2006.
[27] G. Angeles, *Fundamentals of Robotic Mechanical Systems: Theory, Methods, and Algorithms*, 3rd ed. New York: Springer, 2006.
[28] K. Parsa, T. A. Lasky, and B. Ravani, "Design and implementation of a mechatronic, all-accelerometer inertial measurement unit," *IEEE/ASME Trans. Mechatronics*, vol. 12, no. 6, pp. 640–650, Dec. 2007.
[29] K. Parsa, "Dynamics, state estimation, and control of manipulators with rigid and flexible subsystems," Ph.D. dissertaion, Dept. Mech. Eng., McGill Univ., Montreal, QC, Canada, 2003..
[30] (2010). *Analog Devices ADXL330 accelerometer datasheet.* [Online]. Available: http://www.analog.com/en/sensors/inertial-sensors/adxl330/products/product.html.
[31] (2010). *Analog Devices ADXRS610 gyroscope datasheet.* [Online]. Available: http://www.analog.com/en/sensors/inertial-sensors/adxrs610/products/product.html.

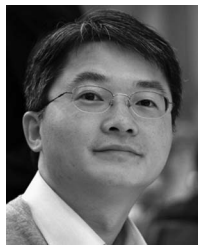

Pei-Chun Lin (S'02–M'05) received the B.S. and M.S. degrees in mechanical engineering from National Taiwan University (NTU), Taipei, Taiwan, in 1996 and 1998, respectively, and the M.S. degree in electrical engineering and computer science and the Ph.D. degree in mechanical engineering from the University of Michigan, Ann Arbor, both in 2005.

From 2005 to 2007, he was a Postdoctoral Research Fellow in the Department of Material Science and Engineering, University of Pennsylvania, Philadelphia. He is currently an Assistant Professor in the Department of Mechanical Engineering, National Taiwan University. His current research interests include bioinspired robotics, mechanical design, sensor design/fusion, control, locomotion, and tunable polymers.

Jau-Ching Lu received the B.S. and M.S. degrees in mechanical engineering from National Taiwan University, Taipei, Taiwan, in 2008 and 2010, respectively.

He is currently a Research Assistant in the Department of Mechanical Engineering, National Taiwan University. His current research interests include inertial measurement units and robot dynamics and control.

Chia-Hung Tsai received the B.S. degree in mechanical engineering from National Cheng Kung University, Tainan, Taiwan, in 2009. He is currently working toward the M.S. degree at National Taiwan University, Taipei, Taiwan.

His current research interests include mobile robots, inertial measurement units, and other sensor applications.

Chi-Wei Ho received the B.S. degree in mechanical engineering from National Chung Hsing University, Taichung, Taiwan, in 2007, and the M.S. degree in mechanical engineering from National Taiwan University, Taipei, Taiwan, in 2009.

He was with Foxconn, Kunshan, China. He is currently an Application Engineer in the Department of Automation Development, HTC, Taoyuan, Taiwan. His current research interests include inertial measurement units and sensor applications.